

---

# Extrapolating Phase-Field Simulations in Space and Time with Purely Convolutional Architectures

---

Anonymous Author(s)

Affiliation

Address

email

## Abstract

Phase-field models of liquid metal dealloying (LMD) can resolve rich microstructural dynamics but become intractable for large domains or long time horizons. We present a conditionally parameterized, fully convolutional U-Net surrogate that generalizes far beyond its training window in both space and time. The design integrates convolutional self-attention and physics-aware padding, while parameter conditioning enables variable time-step skipping and adaptation to diverse alloy systems. Although trained only on short, small-scale simulations, the surrogate exploits the translational invariance of convolutions to extend predictions to much longer horizons than traditional solvers. It accurately reproduces key LMD physics, with relative errors typically under 5% within the training regime and below 10% when extrapolating to larger domains and later times. The method accelerates computations by up to 16,000 times, cutting weeks of simulation down to seconds, and marks an early step toward scalable, high-fidelity extrapolation of LMD phase-field models.

## 1 Introduction

Machine learning has become a powerful tool for accelerating simulations governed by partial differential equations (PDEs), enabling surrogates that run orders of magnitude faster than traditional solvers [12, 29, 18, 19, 15, 6, 7]. Much prior work, however, targets *simplified problems* where large training datasets are reasonably cheap to generate. In such cases, models are trained on complete simulations and rarely tested under conditions far beyond the training data.

Here, we investigate phase-field simulations of liquid-metal de-alloying (LMD) [10, 16, 17, 3, 13, 4], where creating an ideal dataset would require years of high-performance computing time. Phase field simulations for LMD are governed by physically-derived PDEs and can be used to model microstructure and morphology evolution of material systems [9, 11, 33]. We focus on binary alloys in contact with a corrosive liquid, and use a thermokinetic parameterization that triggers rapid selective dissolution from the binary alloy and leads to formation of fine-scale, porous microstructures. The de-alloyed microstructures exhibit a wide variety of nano-scale morphological patterns that ultimately control macro-scale properties, such as material strength. While traditional phase-field solvers can simulate LMD [10, 16, 17, 3, 13, 4], they are limited to short durations and small domains, preventing direct numerical simulations (DNS) from reaching the spatial and temporal scales required in practice.

This scarcity of data is problematic for common machine learning approaches to PDE forecasting, particularly auto-regressive methods [15, 18, 20, 8, 30], which evolve systems step by step, feeding predictions back as inputs. These methods tend to accumulate errors over long horizons. In simple problems, abundant long sequences help mitigate instability, but for LMD only short sequences

36 are available, and models must remain stable when extrapolated far beyond training. Prior LMD  
37 surrogates, such as U-AFNO [5], while promising, lacked this extrapolation capability.

38 To overcome these challenges, we design a modified U-Net [32] surrogate that exploits the translation  
39 invariance of convolutions to handle variable domain sizes while preserving physical consistency. The  
40 architecture uses parametric conditioning [23] to adapt to different alloy and simulation parameters,  
41 and circular padding to strictly enforce boundary conditions. This design ensures stability in long  
42 auto-regressive roll-outs and scales to domains and horizons much larger than those seen in training.  
43 Our model is trained on short simulations over square domains, but during surrogate predictions,  
44 it dynamically extends domain height as corrosion progresses and the corrosive bath sinks into the  
45 alloy, enabling extrapolation in both space and time.

## 46 2 Phase-Field Model for Liquid Metal De-alloying

47 The phase-field model simulates LMD in a binary alloy [10, 3], resolving both the diffuse solid-liquid  
48 interface  $\phi$  and the mole fractions of alloy species  $c_A$ ,  $c_B$ , and  $c_C$  (A and B are part of the alloy, and C  
49 is the corrosive agent. Since  $c_C = 1 - c_A - c_B$ , we only track A and B). The interface and conserved  
50 species dynamics are governed by coupled modified Allen-Cahn and Cahn-Hilliard equations:

$$\frac{\partial \phi}{\partial t} = -\tilde{M}_\phi \frac{\pi^2}{8\eta} \frac{\delta F}{\delta \phi} \quad \frac{\partial c_i}{\partial t} = \nabla \cdot \sum_{j=A,B} M_{ij}(\phi) \nabla \left( \frac{\delta F}{\delta c_j} \right), \quad i \in \{A, B\} \quad (1)$$

51 where  $F$  is the free energy functional containing both interface and bulk chemical contributions.  
52 Ultimately, equation 1 relies on fourth-order spatial derivative terms, and is numerically stiff. Con-  
53 ventional time-integrators require an extremely small time step of  $\Delta t = 10^{-12}$  s to maintain stability  
54 [3, 13]. This makes direct simulation over realistic timescales computationally infeasible, motivating  
55 the use of auto-regressive surrogate models that can leap over many solver steps at once, while  
56 preserving the ability to predict long-term system evolution.

## 57 3 U-Net Surrogate

58 U-Nets [32] are residual convolutional neural networks with a U-shaped encoder-decoder structure  
59 linked by skip connections, enabling efficient gradient propagation and accurate tensor-to-tensor  
60 regression. Originally developed for biomedical segmentation, they are now widely used for PDE-  
61 based physical simulations, particularly in autoregressive prediction where they map spatial input  
62 fields to future states [25, 26, 23, 24]. While not resolution invariant like neural operators [18, 19],  
63 their convolutional locality allows training on small domains and applying to larger ones at fixed  
64 resolution. Outputs are passed through a sigmoid to enforce the [0,1] bounds of the phase and species  
65 fields. We use a conditional U-Net inspired by [23], where parameters modulate the network via  
66 a fully connected conditioning module. The conditioning inputs are the time span between U-Net  
67 input and output, and the reference concentration  $c_A$ . These pass through two hidden layers of 128  
68 neurons with SiLU activation, followed by five linear layers producing scaling vectors of sizes 32,  
69 64, 128, 256, and 512. Vectors are applied to the corresponding U-Net feature channels before skip  
70 concatenation, enabling multi-step predictions and adaptation to varying material conditions without  
71 retraining. The U-Net architecture is shown in figure 1

72 We integrate spatial self-attention in the bottleneck to capture long-range dependencies, building  
73 on prior work that used Vision Transformers (ViTs) in U-Net bottlenecks [5, 27, 25]. Rather than  
74 adopting the full transformer architecture (with fixed-size linear layers constraining input-output  
75 dimensions), we retain only the attention layers [2], implemented entirely with convolutions to  
76 preserve resolution flexibility and allow application to domains larger than those seen in training.  
77 Queries, keys, and values are computed with  $1 \times 1$  convolutions, with query/key channels set to  
78  $1/8^{\text{th}}$  of the input dimension. The U-Net convolutional layers employ  $3 \times 3$  kernels, so padding is  
79 needed to preserve spatial dimensions. Instead of standard zero-padding, which ignores physics, we  
80 design boundary-aware padding [1, 31]. Horizontally, we use circular padding, which hard-enforces  
81 periodic boundary conditions by wrapping left and right edges onto each other. At the top we  
82 apply zero-padding, since both phase and species fields vanish there, and at the bottom we replicate  
83 boundary values to reflect constant composition. This embeds known boundary behaviors directly  
84 into the network, improving accuracy and generalization.

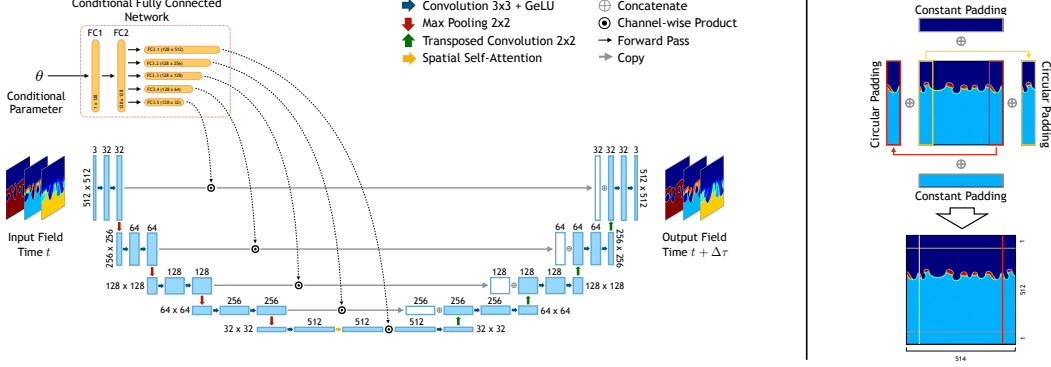


Figure 1: Left: U-Net Architecture. The model takes as input the field at time  $t$  and outputs the field at a future time step  $t + \Delta\tau$  and is conditioned on  $\theta$ . Right: Circular padding for the U-Net convolutions (widths of the padded vectors are exaggerated for illustration).

## 85 4 Training and Testing

86 The training dataset contains simulations with reference  $c_A$  concentrations from 0.20 to 0.40 in 0.05  
 87 increments (1,280 snapshots per concentration). Data is generated on a  $512 \times 512$  grid, depicting  
 88 species C sinking through the A–B alloy toward the lower boundary. Besides  $c_A$ , the model is  
 89 designed to skip 50,000–100,000 time steps per iteration and is implemented in PyTorch [28]. It is  
 90 trained with relative  $\mathcal{L}_2$  loss (common in neural-operator models [18, 19, 5]), Adam optimization [14],  
 91 and a  $10^{-4}$  learning rate, for 80 epochs. Training on a single A100 GPU requires 59 hours. Surrogate  
 92 tests use an auto-regressive roll-out, recursively feeding predictions back as inputs [5, 23]. Leveraging  
 93 U-Net’s convolutional design, we run extended domains twice as tall as training ( $1024 \times 512$ ) to  
 94 capture deeper species C penetration, and extrapolate to horizons about  $3 \times$  longer than in training.  
 95 This domain size is chosen as the largest possible in the limit of computational feasibility, since  
 96 generating DNS test data at  $1024 \times 512$  can take weeks/months on 64–128 CPU cores.  
 97 Because the physics is highly chaotic [3], the surrogate cannot reproduce exact microstructures.  
 98 Instead, the goal is to capture invariant physical trends across simulations [5, 23, 15]. Accuracy is  
 99 defined by recovering key quantities of interest (QoIs) extracted from predicted fields rather than the  
 100 fields themselves. QoIs include interface curvature and perimeter, C penetration depth, remaining A  
 101 and B volumes, and average ligament height [22, 36, 35, 34, 17, 21, 5]. Surrogate QoIs are compared  
 102 against DNS using relative  $\mathcal{L}_2$  error.

## 103 5 Results

104 Figure 2 shows test simulations for  $c_A = 0.2$ , comparing U-Net predictions with the corresponding  
 105 DNS. Both sets of fields illustrate the evolution of species A and B, with the phase-field interface  $\phi$   
 106 outlined in black. Note that the surrogate simulations start at  $t = 0.5\mu\text{s}$ . This is because at  $t = 0\mu\text{s}$ ,  
 107 the initial interface is perfectly flat. Such an initial condition is not directly suitable for the U-Net,  
 108 so we initially run the numerical solver for  $0.5\mu\text{s}$  to initialize the surrogate. Because the system  
 109 is highly chaotic, the predicted microstructures inevitably diverge in detail from the true ones over  
 110 long time horizons. Nevertheless, the surrogate reproduces the key physics: species C penetrates the  
 111 alloy at the correct pace, the interface shifts downward realistically, and the curvature of the interface  
 112 aligns closely with that of the true fields. The ligament structures also form and evolve in a physically  
 113 consistent way, including the characteristic spikes in species A near the interface and the erosion of  
 114 species B. Importantly, the surrogate remains numerically stable, producing no unphysical artifacts,  
 115 even deep into the extrapolation regime. Predictions continue to unroll smoothly, preserving the  
 116 correct physical trends well beyond the training window. Note that here, *training regime* only refers  
 117 to the time span used in the training data, while the surrogate is being compared with completely new  
 118 and independent testing data.

119 Figure 3 reports QoI relative errors in both the training and extrapolation regimes, comparing surrogate  
 120 performance with and without circular padding. Errors in the training regime remain below 5%, and

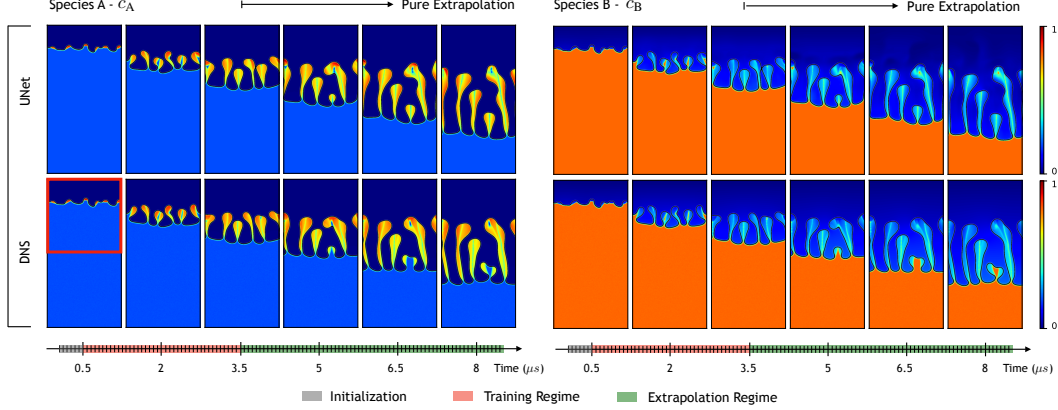


Figure 2: Concentration fields for species A and B. The reference (pre-dealloying) concentration for A is  $c_A = 0.2$ . For each species, the top row represents the U-Net surrogate prediction, and the lower row is the corresponding direct numerical simulation (DNS). The red box illustrates the size of the domain used in the training data.

even during extrapolation it typically stays within 10%. The mean ligament height proves the most difficult QoI to predict. Removing periodic convolutions tends to worsen accuracy, particularly in extrapolation, as mismatched lateral boundaries introduce instabilities and unphysical artifacts in the QoIs. We also benchmark our surrogate against U-AFNOs, a recent surrogate for LMD simulations presented in Bonneville et al. [5]. In this case, the comparison is restricted to  $c_A = 0.3$  and within the training regime, since the earlier approach in [5] cannot handle other concentrations or domain extrapolation. Overall, our surrogate achieves up to 5% better accuracy across most QoIs.

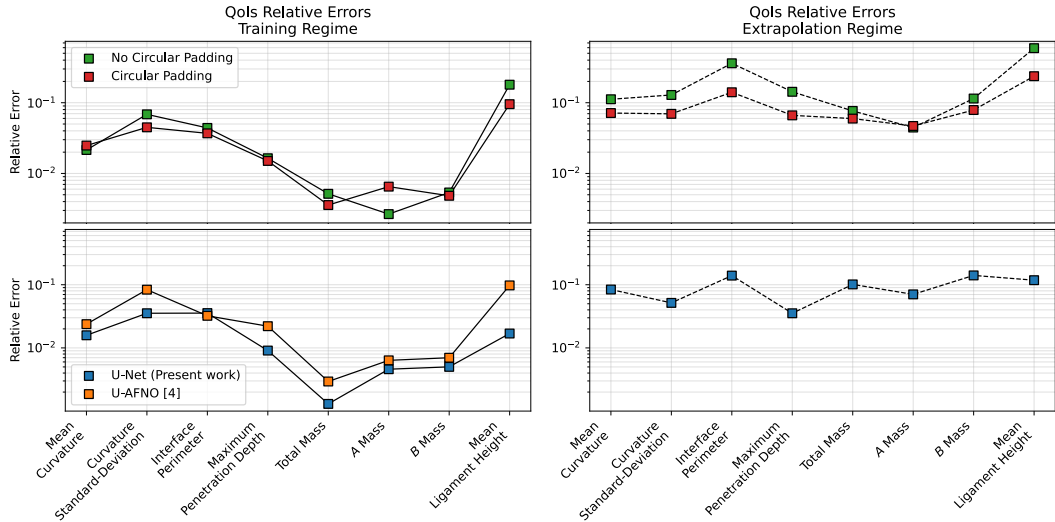


Figure 3: QoIs relative errors. Top row: Errors for the U-Net with and without circular padding (averaged across all tested concentration for  $c_A \in [0.2, 0.4]$ ). Bottom row: The present model (U-Net) performance vs. U-AFNO [5], for  $c_A = 0.3$  (note that the U-AFNO cannot extrapolate).

In conclusion, our surrogate demonstrates the ability to extrapolate at least three times beyond the training horizon, enabled by its fully convolutional design and robust enforcement of boundary conditions. The model delivers both high accuracy and long-term stability. For context, a reference simulation such as the one shown in Figure 2 requires approximately 7.5 days of computation, whereas our surrogate reaches the same time horizon in just 38.5 seconds on a single A100 GPU, a speed up of about 16,000 times.

134 **References**

- 135 [1] Antonio Alguacil, Wagner Gonçalves Pinto, Michael Bauerheim, Marc C. Jacob, and Stéphane  
136 Moreau. Effects of boundary conditions in fully convolutional networks for learning spatio-  
137 temporal dynamics, 2021.
- 138 [2] Dzmitry Bahdanau, Kyunghyun Cho, and Yoshua Bengio. Neural machine translation by jointly  
139 learning to align and translate. 2016.
- 140 [3] Nathan Bieberdorf, Mark Asta, and Laurent Capolungo. Grain boundary effects in high-  
141 temperature liquid-metal dealloying: a multi-phase field study. *npj Computational Materials*, 9,  
142 07 2023.
- 143 [4] Nathan Bieberdorf, Laurent Capolungo, and Mark Asta. Morphologies of dealloying corrosion  
144 attack at grain boundaries. *Acta Materialia*, 297:121308, 2025.
- 145 [5] Christophe Bonneville, Nathan Bieberdorf, Arun Hegde, Mark Asta, Habib N. Najm, Laurent  
146 Capolungo, and Cosmin Safta. Accelerating phase field simulations through a hybrid adaptive  
147 fourier neural operator with u-net backbone. *npj Computational Materials*, 11(1), 01 2025.
- 148 [6] Christophe Bonneville, Youngsoo Choi, Debojyoti Ghosh, and Jonathan L. Belof. Gplasdi:  
149 Gaussian process-based interpretable latent space dynamics identification through deep autoen-  
150 coder. *Computer Methods in Applied Mechanics and Engineering*, 418:116535, 2024.
- 151 [7] Christophe Bonneville, Xiaolong He, April Tran, Jun Sur Park, William Fries, Daniel A.  
152 Messenger, Siu Wun Cheung, Yeonjong Shin, David M. Bortz, Debojyoti Ghosh, Jiun-Shyan  
153 Chen, Jonathan Belof, and Youngsoo Choi. A comprehensive review of latent space dynamics  
154 identification algorithms for intrusive and non-intrusive reduced-order-modeling. *arXiv preprint*  
155 *arXiv:2403.10748*, 2024.
- 156 [8] Qianying Cao, Somdatta Goswami, and George Em Karniadakis. Lno: Laplace neural operator  
157 for solving differential equations, 2023.
- 158 [9] Long-Qing Chen. Phase-field models for microstructure evolution. *Annual Review of Materials  
159 Research*, 32(Volume 32, 2002):113–140, 2002.
- 160 [10] Pierre-Antoine Geslin, Ian Mccue, Bernard Gaskey, Jonah Erlebacher, and Alain Karma.  
161 Topology-generating interfacial pattern formation during liquid metal dealloying. *Nature  
162 communications*, 6:8887, 11 2015.
- 163 [11] A. Karma. Phase field methods. In K.H. Jürgen Buschow, Robert W. Cahn, Merton C.  
164 Flemings, Bernhard Ilschner, Edward J. Kramer, Subhash Mahajan, and Patrick Veyssi  e,  
165 editors, *Encyclopedia of Materials: Science and Technology*, pages 6873–6886. Elsevier,  
166 Oxford, 2001.
- 167 [12] George Em Karniadakis, Ioannis G. Kevrekidis, Lu Lu, Paris Perdikaris, Sifan Wang, and Liu  
168 Yang. Physics-informed machine learning. *Nature Reviews Physics*, 3(6):422–440, 2021.
- 169 [13] Justin Kerr, Nathan Bieberdorf, Laurent Capolungo, and Mark Asta. Morphology selection in  
170 dealloying: A phase field study of the coupling among kinetic mechanisms. *Phys. Rev. Mater.*,  
171 8:103802, Oct 2024.
- 172 [14] Diederik P. Kingma and Jimmy Ba. Adam: A method for stochastic optimization, 2017.
- 173 [15] Nikola B. Kovachki, Zongyi Li, Burigede Liu, Kamyar Azizzadenesheli, Kaushik Bhattacharya,  
174 Andrew M. Stuart, and Anima Anandkumar. Neural operator: Learning maps between function  
175 spaces. *CoRR*, abs/2108.08481, 2021.
- 176 [16] Longhai Lai, Bernard Gaskey, Alyssa Chuang, Jonah Erlebacher, and Alain Karma. Topological  
177 control of liquid-metal-dealloyed structures. *Nature Communications*, 13(1):2918, 2022.
- 178 [17] Longhai Lai, Pierre-Antoine Geslin, and Alain Karma. Microstructural pattern formation during  
179 liquid metal dealloying: Phase-field simulations and theoretical analyses. *Phys. Rev. Mater.*,  
180 6:093803, Sep 2022.

- 181 [18] Zongyi Li, Nikola Kovachki, Kamyar Azizzadenesheli, Burigede Liu, Kaushik Bhattacharya,  
 182 Andrew Stuart, and Anima Anandkumar. Fourier neural operator for parametric partial differen-  
 183 tial equations. 2021.
- 184 [19] Lu Lu, Pengzhan Jin, Guofei Pang, Zhongqiang Zhang, and George Em Karniadakis. Learning  
 185 nonlinear operators via deeponet based on the universal approximation theorem of operators.  
 186 *Nature Machine Intelligence*, 3(3):218–229, March 2021.
- 187 [20] Lu Lu, Pengzhan Jin, Guofei Pang, Zhongqiang Zhang, and George Em Karniadakis. Learning  
 188 nonlinear operators via deeponet based on the universal approximation theorem of operators.  
 189 *Nature Machine Intelligence*, 3(3):218–229, March 2021.
- 190 [21] Ian McCue, Bernard Gaskey, Pierre-Antoine Geslin, Alain Karma, and Jonah Erlebacher.  
 191 Kinetics and morphological evolution of liquid metal dealloying. *Acta Materialia*, 115:10–23,  
 192 2016.
- 193 [22] Ian McCue, Alain Karma, and Jonah Erlebacher. Pattern formation during electrochemical and  
 194 liquid metal dealloying. *MRS Bulletin*, 43(1):27–34, 2018.
- 195 [23] Vivek Oommen, Khemraj Shukla, Saaketh Desai, Remi Dingreville, and George Em Karniadakis.  
 196 Rethinking materials simulations: Blending direct numerical simulations with neural operators,  
 197 2023.
- 198 [24] Vivek Oommen, Khemraj Shukla, Somdatta Goswami, Remi Dingreville, and George Karni-  
 199 adakis. Learning two-phase microstructure evolution using neural operators and autoencoder  
 200 architectures. *npj Computational Materials*, 8, 09 2022.
- 201 [25] Oded Ovadia, Adar Kahana, Panos Stinis, Eli Turkel, and George Em Karniadakis. Vito: Vision  
 202 transformer-operator, 2023.
- 203 [26] Oded Ovadia, Vivek Oommen, Adar Kahana, Ahmad Peyvan, Eli Turkel, and George Em  
 204 Karniadakis. Real-time inference and extrapolation via a diffusion-inspired temporal transformer  
 205 operator (ditto). 2023.
- 206 [27] Oded Ovadia, Vivek Oommen, Adar Kahana, Ahmad Peyvan, Eli Turkel, and George Em  
 207 Karniadakis. Real-time inference and extrapolation via a diffusion-inspired temporal transformer  
 208 operator (ditto), 2023.
- 209 [28] Adam Paszke, Sam Gross, Francisco Massa, Adam Lerer, James Bradbury, Gregory Chanan,  
 210 Trevor Killeen, Zeming Lin, Natalia Gimelshein, Luca Antiga, Alban Desmaison, Andreas  
 211 Köpf, Edward Yang, Zach DeVito, Martin Raison, Alykhan Tejani, Sasank Chilamkurthy,  
 212 Benoit Steiner, Lu Fang, Junjie Bai, and Soumith Chintala. Pytorch: An imperative style,  
 213 high-performance deep learning library, 2019.
- 214 [29] Maziar Raissi, Paris Perdikaris, and George Em Karniadakis. Physics informed deep learning  
 215 (part i): Data-driven solutions of nonlinear partial differential equations, 2017.
- 216 [30] Bogdan Raonić, Roberto Molinaro, Tim De Ryck, Tobias Rohner, Francesca Bartolucci, Rima  
 217 Alaifari, Siddhartha Mishra, and Emmanuel de Bézenac. Convolutional neural operators for  
 218 robust and accurate learning of pdes, 2023.
- 219 [31] Pu Ren, Chengping Rao, Yang Liu, Jian-Xun Wang, and Hao Sun. Phycrnet: Physics-informed  
 220 convolutional-recurrent network for solving spatiotemporal pdes. *Computer Methods in Applied  
 221 Mechanics and Engineering*, 389:114399, February 2022.
- 222 [32] Olaf Ronneberger, Philipp Fischer, and Thomas Brox. U-net: Convolutional networks for  
 223 biomedical image segmentation. 2015.
- 224 [33] Ingo Steinbach. Phase-field models in materials science. *Modelling and Simulation in Materials  
 225 Science and Engineering*, 17(7):073001, jul 2009.
- 226 [34] Anh Tran, Dehao Liu, Hoang Tran, and Yan Wang. Quantifying uncertainty in the process-  
 227 structure relationship for al-cu solidification. *Modelling and Simulation in Materials Science  
 228 and Engineering*, 27(6):064005, jun 2019.

229 [35] Samad Vakili, Ingo Steinbach, and Fathollah Varnik. On the numerical evaluation of local  
230 curvature for diffuse interface models of microstructure evolution. *Procedia Computer Science*,  
231 108:1852–1862, 2017. International Conference on Computational Science, ICCS 2017, 12-14  
232 June 2017, Zurich, Switzerland.

233 [36] Takeshi Wada, Pierre-Antoine Geslin, Daixu Wei, and Hidemi Kato. Partial liquid metal  
234 dealloying to synthesize nickel-containing porous and composite ferrous and high-entropy  
235 alloys. *Communications Materials*, 4(1):43, December 2023.